Quantitative Proteomic and Phosphoproteomic Approaches for Deciphering the Signaling Pathway for Tension Wood Formation in Poplar

ARTICLE *in* JOURNAL OF PROTEOME RESEARCH · JUNE 2015

Impact Factor: 4.25 · DOI: 10.1021/acs.jproteome.5b00140 · Source: PubMed

10 AUTHORS, INCLUDING:

Jean-Charles Leplé

French National Institute for Agricultural Rese…

98 PUBLICATIONS **4,132** CITATIONS

SEE PROFILE

Nicolas Richet

Université catholique de Louvain

12 PUBLICATIONS **44** CITATIONS

SEE PROFILE

Marc Bonneu

Bordeaux INP

67 PUBLICATIONS **1,574** CITATIONS

SEE PROFILE

Christophe Plomion

French National Institute for Agricultural Rese…

226 PUBLICATIONS **5,574** CITATIONS

SEE PROFILE

Journal of proteome research

Article

pubs.acs.org/jpr

Quantitative Proteomic and Phosphoproteomic Approaches for Deciphering the Signaling Pathway for Tension Wood Formation in Poplar

Mélanie Mauriat,[†,‡] Jean-Charles Leplé,[§] Stéphane Claverol,[⊥] Jérôme Bartholomé,[†,‡] Luc Negroni,[⊥] Nicolas Richet,[§] Céline Lalanne,[†,‡] Marc Bonneu,[⊥] Catherine Coutand,[¶,∥] and Christophe Plomion*[,†,‡]

[†]INRA, UMR 1202 BIOGECO, F-33610 Cestas, France

[‡]Univ. Bordeaux, BIOGECO, UMR1202, F-33615 Pessac, France

[§]INRA, UR0588 AGPF, 2163 Avenue de la Pomme de Pin, CS 40001 Ardon, F-45075 Orléans Cedex 2, France

[⊥]Plateforme Protéome, CGFB, Université Bordeaux Segalen, F-33076 Bordeaux, France

[¶]INRA, UMR 547 PIAF, 234 Avenue du Brézet, F-63100 Clermont-Ferrand, France

[∥]Clermont Université, Université Blaise Pascal, UMR 547 PIAF, F-63100 Clermont-Ferrand, France

Supporting Information

ABSTRACT: Trees adjust their growth following forced changes in orientation to re-establish a vertical position. In angiosperms, this adjustment involves the differential regulation of vascular cambial activity between the lower (opposite wood) and upper (tension wood) sides of the leaning stem. We investigated the molecular mechanisms leading to the formation of differential wood types through a quantitative proteomic and phosphoproteomic analysis on poplar subjected to a gravitropic stimulus. We identified and quantified 675 phosphopeptides, corresponding to 468 phosphoproteins, and 3 763 nonphosphorylated peptides, corresponding to 1 155 proteins, in the differentiating xylem of straight-growing trees (control) and trees subjected to a gravitational stimulus during 8 weeks. About 1% of the peptides were specific to a wood type (straight, opposite, or tension wood). Proteins quantified in more than one type of wood were more numerous: a mixed linear model showed 389 phosphopeptides and 556 proteins to differ in abundance between tension wood and opposite wood. Twenty-one percent of the phosphoproteins identified here were described in their phosphorylated form for the first time. Our analyses revealed remarkable developmental molecular plasticity, with wood type-specific phosphorylation events, and highlighted the involvement of different proteins in the biosynthesis of cell wall components during the formation of the three types of wood.

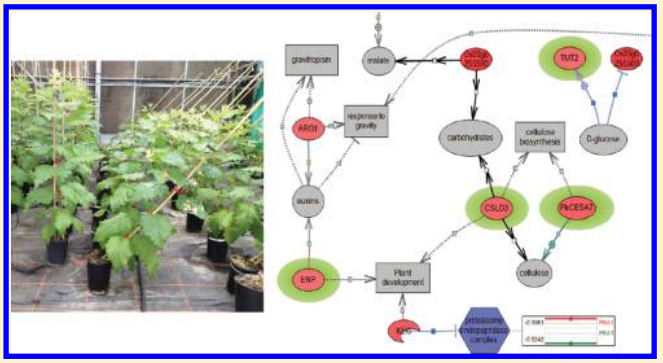

KEYWORDS: *wood formation, tension wood, phosphoproteomics, proteomics, poplar, cell wall*

INTRODUCTION

In nature, trees must adapt to changes in their environment to maintain optimal growth. Strong winds, heavy wet snow, and unstable soils may result in a deviation from the vertical position. Trees respond to such gravitropic disturbances by reorienting their stem along the vector of gravity. The apical part of the stem (which is still elongating) bends back toward a vertical position through faster growth on one side of the stem. By contrast, the bending of sections displaying secondary thickening is achieved by modification of the type of wood produced by the cambium on either side of the trunk, which results in asymmetric growth of the stem and modifications to the forces exerted within the stem.[1] In angiosperms, the wood formed on the upper side of an inclined stem is called tension wood (TW), and that formed on the lower side is called opposite wood (OW). TW may be seen as analogous to the "muscle" of trees because it presents a very high tensile stress (greater than that of OW or straight wood (SW)), which enables it to reorient the stem toward a vertical position.[2] The asymmetric nature of wood formation and the occurrence of nonuniform mechanical stresses around the tree circumference result in differences in the physical and mechanical properties of opposite sides of the stem. These differences result in contrasting wood distortion, strength, and workability properties between the two sides of the stem, which have major consequences for the wood processing industry.

The morphology, anatomy, and ultrastructure of TW and its differences from SW and OW have been described in detail (reviewed in ref 3). The proportions of the different wood cell

Received: February 14, 2015
Published: June 26, 2015

DOI: 10.1021/acs.jproteome.5b00140
J. Proteome Res. 2015, 14, 3188−3203

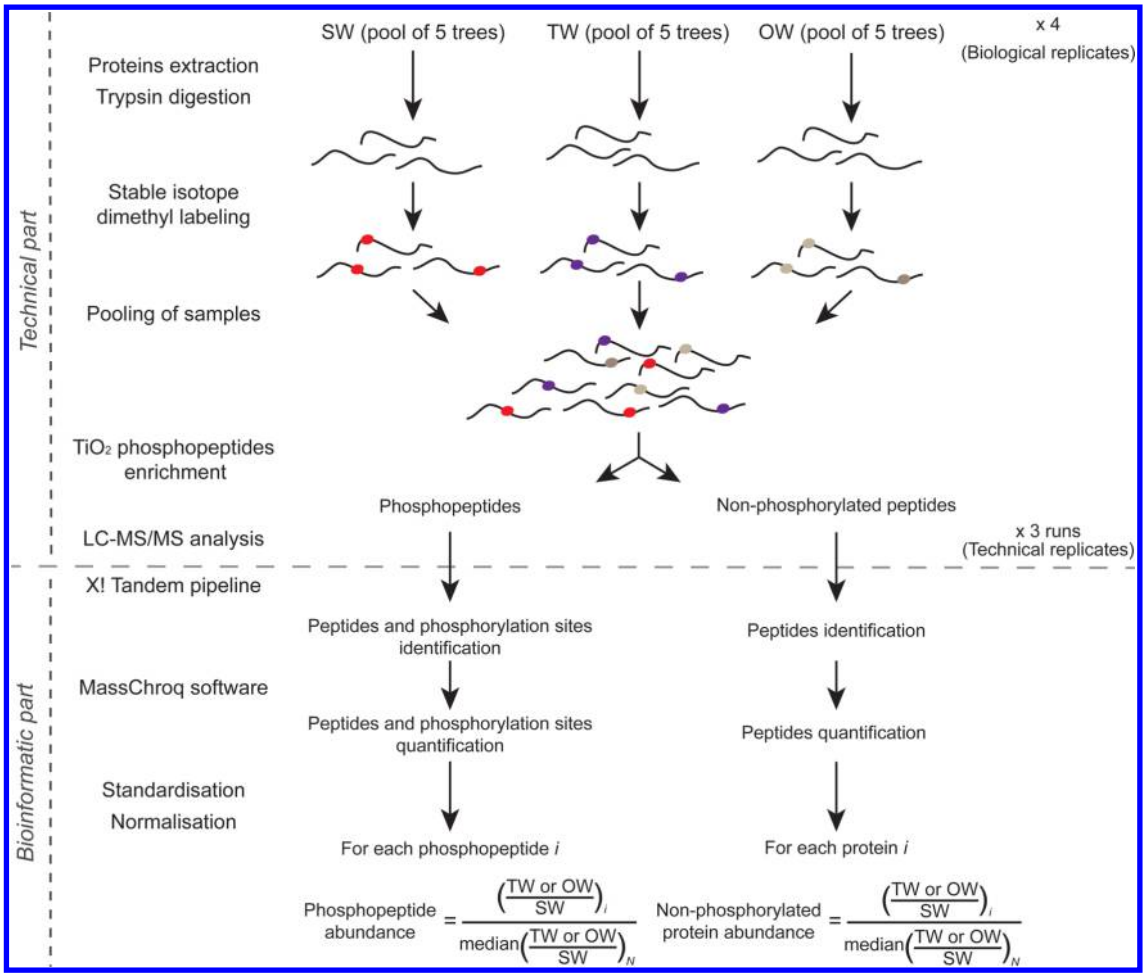

Figure 1. Overview of the experimental procedure used for phosphoproteome and global proteome analyses of poplar wood-forming tissue. Each biological replicate corresponded to a pool of five saplings. TW and OW peptide abundances (i) were calculated relative to those in SW, which was used as a standard proteome with normalization against the median of the corresponding ratios of all the peptides (N) of the liquid chromatography tandem mass spectrometry (LC−MS/MS) run.

types differ between TW and SW. Indeed, vessel density and diameter have been found to be smaller in the TW than in the SW of many angiosperm trees. The smaller diameter of the vessels results from a smaller lumen area rather than a change in wall structure.[4] Axial parenchyma also seems to be less abundant and rays more abundant in TW.[4] Conflicting data have been obtained concerning fibers: the differences in fiber length and diameter between TW and SW appear to be species-specific.[3] However, area of fiber is always larger in TW side mostly because of a greater cambial activity but also because of a decrease of vessel density. Moreover, TW fibers have a particular structure. The TW of many species contains an unusual form of fiber, the gelatinous fiber (G-fiber), so-called because of the presence of a gelatinous layer in the cell wall. The secondary walls of normal fibers consist of three layers (S1, S2, and S3), whereas those of TW fibers contain variable numbers of S-layers, generally with a gelatinous (G)-layer on the innermost side of the cell wall. The thickness of the G-layer is correlated with the tensile stress of the TW. The gelatinous appearance of these fibers results from the presence of a large proportion of cellulose in the G-layer. It was long thought that this layer consisted almost entirely of cellulose, but it is now clear that many other compounds are present in this layer. These compounds include lignin, hemicellulose, xyloglucan, pectin, rhamnogalacturonan, and arabinogalactan.[5] Both the proportions of these compounds and their arrangement in the various layers of the cell wall differ between TW and SW (reviewed in ref 6). The microfibril angle is smaller (almost parallel to the fiber axis) in G-layers than in the S-layers, and cellulose crystallinity is greater in G-layers than in S-layers. TW fibers also have a lower lignin content and a higher lignin−subunit (syringyl/guaiacyl) ratio.

Comparative studies based on transcriptomics,[7,8] proteomics,[9,10] or metabolomics[8] have elucidated some of the differences between the biosynthesis pathways operating in TW, SW, and OW cell wall formation, but the molecular mechanisms involved have yet to be fully characterized. These and other studies have provided information about the regulation of these mechanisms with the detection of several transcription factors. In particular, the NAC and MYB transcription factor families are known to play a major role in the transition from primary to secondary cell wall formation, and some of these factors (together with several others that have yet to be functionally analyzed) may be involved in the transition from S-to-G-layer formation.[6]

However, the global signaling pathway underlying gravitropism remains unclear. It has been suggested that a cascade of protein phosphorylation and dephosphorylation occurs during gravitropism. Indeed, these post-translational modifications,

DOI: 10.1021/acs.jproteome.5b00140
J. Proteome Res. 2015, 14, 3188−3203

which are both rapid and reversible, are involved in many stress response signaling cascades.

In this study, we induced the gravitropic response and the formation of TW and OW by tilting poplar trees at an angle of 35° from the vertical position. We combined quantitative proteomic and phosphoproteomic analysis to decipher the molecular actors of the gravitropic response with a focus on phosphorylation events linked to differential wood formation. With this approach, we were able to characterize and quantify 675 unique phosphopeptides corresponding to 468 phosphoproteins and 3 763 nonphosphorylated peptides corresponding to 1 155 proteins. Analysis of these two data sets revealed wood type-specific phosphorylation events and confirmed the presence of different protein families potentially involved in the differentiation of TW, OW, and SW.

MATERIALS AND METHODS

Plant Material

The plant material was grown at INRA Orléans (France). Forty poplar (*Populus tremula* x *Populus alba*, accession INRA #717−1B4) saplings grown *in vitro* were allowed to acclimate for 3 weeks in a mini-greenhouse and were then transplanted into 4 L pots individually supplied by a strip system with water containing 0.5 g L^{-1} fertilizers (NPK 18−11−18, Universol Blue). After 6 weeks, the saplings had reached a height of about 60 cm. Half the saplings were artificially tilted, at 35° from the vertical, with a rigid stick, which was reattached weekly to maintain an early gravitropic signal. The other saplings (controls) were allowed to grow straight (Figure S1A, Supporting Information). After 8 weeks of growth, we harvested 40 cm-long stem fragments from the collar of the plant. These fragments were cut in two longitudinally, through the pith, and their bark was removed (Figure S1B, Supporting Information). The developing xylem was scraped off to obtain SW-forming tissue (from the control plants), TW-, and OW-forming tissues (from the tilted plants), which were stored at −80 °C until use. Photomicrographs of stem cross-sections were obtained after staining with safranin O/Astra blue to attest the presence of G-fiber in the TW sample, and its absence in the SW and OW samples, while fibers, ray cells, and vessels were present in the three samples (Figure S1C−H, Supporting Information).

Protein Extraction

The work flow from extraction to the estimation of protein abundance is described in Figure 1. Proteins were extracted from pools of five plants, with four biological replicates per type of wood (TW, OW, and SW). Proteins were extracted from 1.6 g of finely ground developing xylem, as previously described[11] but with an additional step in which proteins were solubilized by incubation in 1% sodium dodecyl sulphate (SDS) under shaking for 1 h at 4 °C. The resulting solution was centrifuged for 15 min at 16 000 × *g* and 4 °C. The supernatant was mixed with a solution of trichloroacetic acid (TCA) in 100% acetone to obtain a final concentration of 15% TCA, and the resulting mixture was incubated for 1 h at 4 °C. The mixture was then centrifuged for 20 min at 16 000 × *g* and 4 °C; the pellet was washed twice in *β*-mercaptoethanol in acetone and then dried at room temperature. The protein pellet was resolubilized in 6 M urea, 2 M thiourea, 4% Chaps, and 10 mM DTT, and the resulting solution was stored at −80 °C.

Trypsin Digestion

For each sample (a pool of five plants), an amount of solution corresponding to 1.5 mg of protein was diluted with 50 mM NH_4HCO_3 to obtain a urea/thiourea concentration of 1 M compatible with trypsin digestion. The proteins were alkylated by mixing with 4% 1 M IAA 100 mM NH_4HCO_3 and incubating for 1 h at 4 °C. Proteins were digested with trypsin (dimethylated trypsin from porcin pancreas, Sigma-Aldrich, Saint-Louis, USA) at an enzyme/substrate ratio of 1:100 by incubation overnight at 37 °C with shaking. The reaction was stopped by adding 1% formic acid. The peptides were then dried under vacuum.

Peptide Labeling

Tryptic peptides were stably labeled by reductive amination.[12] The SW samples were labeled with formaldehyde CH_2O (light label); the TW samples were labeled with formaldehyde CD_2O (intermediate label); and the OW samples were labeled with formaldehyde $^{13}CD_2O$ and sodium cyanoborodeuteride $NaBD_3CN$ (heavy label). Dried peptides were resuspended in 1 mL of 5% formic acid and loaded onto a SepPak C18 cartridge column (3 cc; Waters, Saint-Quentin en Yvelines, France). The peptides were labeled with the appropriate reagent (light, intermediate, and heavy) over a period of 10 min on the column. Labeled peptides were eluted from the columns in 0.6% acetic acid, 80% acetonitrile. The three samples corresponding to the same biological replicate were then pooled before drying under vacuum.

Phosphopeptide Enrichment with TiO_2

We used a TiO_2 column (2 × 50 mm^2) to separate the nonretained fraction containing mostly nonphosphopeptides from the eluted fraction containing most of the phosphopeptides. The peptide mixtures were resolubilized in 5% trifluoroacetic acid, 1 M glycolic acid, and 20% acetonitrile before injection onto the TiO_2 column in a Proteomelab PF2D protein fractionation system (Beckman Coulter, Pasadena, USA). We collected the nonretained fraction and the fraction eluted with 1 M NH_4OH pH 11.7 separately. We added 1% formic acid to each fraction and then evaporated off about half the solvent under vacuum. The two fractions were desalted with SepPak C18 and were then dried under vacuum.

Mass Spectrometry (MS)

The peptide mixtures were analyzed on an Ultimate 3000 nano liquid chromatography (LC) system (Dionex, Sunnyvale, USA) coupled to a nanospray LTQ-Orbitrap XL mass spectrometer (ThermoFinnigan, San Jose, USA). We ran 10 *μ*L of peptide digests (after a 10-fold dilution for the nonretained fraction) on a 300 *μ*m inner diameter (id) × 5 mm C18 PepMapTM trap column (LC Packings, Amsterdam, Netherlands) at 30 *μ*L/min. The peptides were eluted from the trap column onto an analytical 75 mm id × 15 cm C18 Pep-Map column (LC Packings) with a 5−40% linear gradient of solvent B over a period of 225 min (solvent A was 0.1% formic acid in 5% acetonitrile (ACN), and solvent B was 0.1% formic acid in 80% ACN). The flow rate for separation was set at 200 nL/min. The mass spectrometer was used in positive ion mode at a needle voltage of 1.8 kV and a capillary voltage of 12 V. Data were acquired in a data-dependent mode, alternating an Fourier transform MS (FTMS) scan survey over the range m/z 300−1700 and six ion trap tandem mass spectrometry (MS/MS) scans with collision-induced dissociation (CID) as the activation mode. MS/MS spectra were acquired with a 3 m/z

DOI: 10.1021/acs.jproteome.5b00140
J. Proteome Res. 2015, 14, 3188−3203

unit ion isolation window and a normalized collision energy of 35. Monocharged ions and ions with unassigned charge states were rejected from fragmentation. The duration of dynamic exclusion was set at 30 s. Each biological replicate was run three times without exclusion lists (technical replicates) to increase proteome coverage.

Peptide Identification and Quantification

Queries were made with X!Tandem[13] through the X! TandemPipeline 3.3.0 interface against the *Populus trichocarpa* v3.0 data set of 64 266 entries (Phytozome portal, http://www.phytozome.net/). The search parameters were as follows: mass accuracy of the monoisotopic peptide precursor and peptide fragments of 10 ppm and 0.5 Da, respectively. Only b- and y-ions were considered. The oxidation of methionine residues (+16 Da) and the phosphorylation of serine, threonine, and tyrosine residues (+79 Da) were considered as variable modifications. The carbamidomethylation (+57 Da) of cysteine residues and the dimethylation of lysine residues and N-terminus of the peptides, with the light (+28 Da), intermediate (+32 Da), or heavy (+36 Da) form of the labeling reagent, were considered as fixed modifications. One missed trypsin cleavage was allowed. All LC−MS/MS runs were grouped into a single data set and analyzed with MassChroQ software[14] for alignment, peak detection, and quantification.

The proteome obtained for the SW sample was considered to be the standard proteome. Peptide abundances in TW and OW were therefore calculated relative to that in SW. The data were further normalized by dividing each ratio (TW/SW or OW/SW) by the median value of the ratios of each LC−MS/MS run. The normalized ratios were considered to correspond to the relative peptide abundance. The overall "TW/SW"/"OW/SW" ratio, or TW/OW, provided a metric for estimating differences in abundance between the two types of wood (TW and OW) from tilted trees.

Data Analysis

Statistical Analyses. Proteins may have more than one phosphorylation site, not all of which are necessarily phosphorylated simultaneously, and these sites may play different roles. We therefore analyzed phosphopeptides separately, whereas nonphosphopeptides were grouped by protein using the grouping algorithm of the X!tandem pipeline. Proteins identified with at least one common peptide were grouped by functions. These groups gathered together paralogs. For an easier reading of the manuscript, the name of the first protein of the group was used in the discussion. The following models were implemented in R software (http://www.R-project.org/) to assess the effect of wood type (TW or OW) on relative phosphopeptide or protein abundance:

$$Y_{ijk} = \mu + W_i + B_j + W_i \times B_j + \varepsilon_{ijk} \quad (1)$$

and

$$Y_{ijk} = \mu + W_i + B_j + W_i \times B_j + t_k + \varepsilon_{ijk} \quad (2)$$

where Y_{ijk} is the relative phosphopeptide or protein abundance, μ the general mean, and ε_{ijk} the residual random effect $\sim N(O,\sigma^2)$. The first model (1) included wood type (W_i, $i = 2$), biological replicates (B_j, $j = 4$), and their interaction ($W_i \times B_j$) as fixed effects. The second model (2) was a mixed model including technical replicate (t_k, $k = 3$) as a random effect to take into account the variability between technical replicates. We used two different functions from the R software suite: *lm* for model (1) and *lmer* from the lme4 package for model (2). Only phosphopeptides and proteins for which at least eight of the 12 values were available (four biological replicates and three technical replicates) per sample were retained to ensure that the estimates of effects were reliable. We thus excluded 73 phosphopeptides and 200 proteins from the initial data sets. For both models, *p*-values were adjusted for multiple testing with the R function *p.adjust,* by the FDR method.[15] Only phosphopeptides and proteins for which the wood-type effect was significant in both models were retained for subsequent analyses.

Hierarchical Clustering According to the Relative Abundance of Phosphoproteins and Proteins. The abundance of each phosphoprotein was determined by calculating the mean of the normalized values for all the phosphopeptides identified as belonging to the protein. The abundance of proteins (found nonphosphorylated) was determined from the normalized values previously computed for each protein. Hierarchical clustering was performed with EPCLUST software (http://www.bioinf.ebc.ee/EP/EP/EPCLUST/)[16] using a logarithm base 10 transformation of relative protein abundance. The default methods for distance calculation (correlation measure-based distance) and clustering (average linkage, UPGMA) were used.

Gene Ontology and EuKaryotic Orthologous Groups Annotations of Phosphoproteins and Proteins. The Gene Ontology (GO) and EuKaryotic Orthologous Groups (KOG) annotations and the Best Hit *Arabidopsis* obtained for the phosphoproteins and nonphosphorylated proteins were retrieved with the BioMart tool from the Phytozome portal. For phosphoproteins, we used the *Arabidopsis* orthologs of these proteins to screen the P3DB phosphoprotein database (http://www.p3db.org) to determine whether these proteins had already been reported to be phosphorylated in other phosphoproteomic studies.

Characterization of Phosphorylation Sites. Significantly over-represented phosphorylation site motifs were extracted from the list of phosphopeptides with motif-x software[17,18] (http://motif-x.med.harvard.edu/motif-x.html). With this tool, the phosphopeptide sequences must be centered on the phosphorylated residue (serine, threonine, or tyrosine) and must be at least 13 residues long. For phosphopeptides in which the phosphorylated residue was too close to the end of the phosphopeptide to satisfy these conditions, additional residues were added from the sequence from the corresponding gene model. Phosphopeptides with a phosphorylated residue too close to the first or last amino acid of the protein were excluded from the study. For phosphopeptides displaying serine phosphorylation, we retained the default settings of motif-x (i.e., occurrence threshold of 20, *p*-value of 0.000001 for significance), and the IPI *Arabidopsis* Proteome was used as the background. Phosphopeptides displaying threonine phosphorylation were much less numerous. We therefore decreased the occurrence to 3 and the *p*-value for significance to 0.0005 to ensure that some motifs were detected. There were too few phosphopeptides displaying tyrosine phosphorylation to obtain any significant motifs.

Gene Network Analyses. We used the complete lists of regulated and specific phosphoproteins identified to search for subnetworks enriched in these entities using the FNSE function in PathwayStudio[19] with Ariadne Pathway Studio 9 Desktop edition software and the Resnet Plant Version 4 database (Ariadne Genomics Inc., Rockville, MD, USA). The relationships identified were manually curated by inspection of the

DOI: 10.1021/acs.jproteome.5b00140
J. Proteome Res. 2015, 14, 3188−3203

Table 1. Identification and Quantification of Phosphoproteins and Proteins Found Nonphosphorylated from Three Types of Poplar Wood-Forming Tissues: SW, TW, and OW

fraction enriched in phosphopeptides	fraction not enriched in phosphopeptides
776 spectra quantified	4165 spectra quantified
675 unique phosphopeptides (468 phosphoproteins)	3763 unique peptides/1155 proteins
653 unique phosphopeptides common to SW and TW or to SW and OW (452 phosphoproteins)	1112 proteins common to SW and TW or to SW and OW
626 phosphopeptides with a minimum of eight technical replicates per type of wood (431 phosphoproteins)	955 proteins with a minimum of eight technical replicates per type of wood
389 phosphopeptides (293 phosphoproteins) differing in abundance between TW and OW	559 proteins differing in abundance between TW and OW

references, and the expression ratio (TW/OW) of each protein was indicated on a color scale running from red to blue (with red corresponding to higher levels of expression in TW and blue corresponding to higher levels of expression in OW; the intensity of the color being dependent on the absolute value of the ratio).

RESULTS

Identification and Distribution of Phosphopeptides, Phosphoproteins, and Proteins from SW, TW, and OW

Identification of Phosphopeptides and Nonphosphorylated Peptides from the Three Types of Wood. Proteins extracted from the wood-forming tissues of straight poplar saplings (SW) and from the two sides of the inclined stem in bent saplings, TW and OW, were analyzed by LC−MS/MS. Peptides were identified by querying the *Populus trichocarpa* v3.0 data set with the X!Tandem pipeline. We searched for phosphorylation sites and carried out peptide quantification with X!Tandem and MassChroQ, respectively. The fraction enriched in phosphopeptides contained 675 unique phosphopeptides (PPp) corresponding to 468 phosphoproteins (PP) (Table 1). The nonenriched fraction contained 3763 quantified peptides corresponding to 1155 proteins (nonphosphorylated proteins: NPP). The proteins were grouped with the grouping algorithm of the X!tandem pipeline. The groups corresponded to paralogs were impossible to distinguish because of their similarity of sequence blasting the peptides.

Phosphorylation Sites Overrepresented in the Different Types of Wood. In total, we identified 755 phosphorylation sites in the 675 PPp obtained in this study; 88% of the PPp contained one phosphorylated residue, 11% were diphosphorylated, and only 1% contained three phosphorylation sites (Figure 2A). A study of the phosphorylation status of poplar bud proteins[20] reported a higher percentage (93.8%) of monophosphorylated PPp, whereas 81% monophosphorylation was observed for peptides in an *Arabidopsis* cell suspension.[21] These differences in the percentage of monophosphorylated peptides can be explained by the use of different enrichment strategies, which are known to have specific affinities for PPp displaying phosphorylation at one or multiple sites.[22] The higher percentage of PPp phosphorylated at multiple sites obtained in our study than in the study on poplar buds should not be interpreted as indicating a higher complexity of the phosphoproteome in wood than in buds. Instead, it may simply reflect a difference in enrichment strategy or efficiency between the two studies.

Serine was the most frequently phosphorylated amino acid (89.1%) followed by threonine (8.7%) and then tyrosine, which accounted for only 2.2% of the phosphorylated residues (Figure 2B). We therefore found a slightly lower frequency of pSer and a higher frequency of pThr than reported in other plant studies: 81.3% for pSer and 17.4% for pThr in poplar buds,[20] 85.7% for pSer and 13.5% for pThr in maize leaves,[23] or 85% for pSer and 10.6% for pThr in *Arabidopsis* cell suspension.[21] The distribution of phosphorylated residues in TW differed slightly from that in OW ($p < 0.05$) (Figure 2B); the values of OW were more similar to those reported in other studies (83.8% for pSer, 11.6% for pThr, and 4.6% for pTyr). This suggests that TW and OW possess different phosphorylation events.

We analyzed the motifs surrounding the phosphorylated residues to have more arguments converging to this hypothesis. Indeed, these motifs are footprints of kinase activity, so the presence of different motifs in different types of wood could suggest the involvement of different kinases in the correspond-

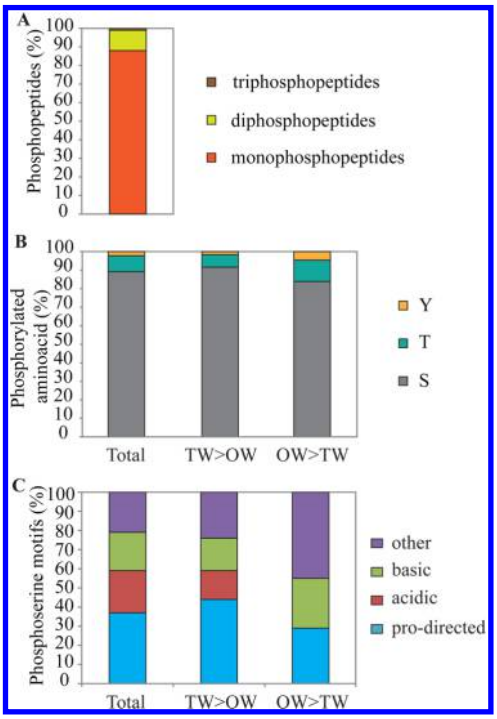

Figure 2. Distribution of phosphorylation sites in the phosphoproteome of poplar wood-forming tissue. (A) Percentages of mono-, di-, and triphosphopeptides identified. (B) Percentages of serine, threonine, and tyrosine residues among the phosphorylated amino acids for all the phosphorylation sites identified, phosphorylation sites more abundant in TW than in OW, and phosphorylation sites more abundant in OW than in TW. (C) Kinase-specific motifs identified with motif-x. Distribution of the various types of phosphoserine motifs among all phosphoserine peptides, the phosphoserine peptides more abundant in TW than in OW, and the phosphoserine peptides more abundant in OW than in TW.

DOI: 10.1021/acs.jproteome.5b00140
J. Proteome Res. 2015, 14, 3188−3203

ing developmental processes even if it is also known that the same kinase can recognize different motifs.[24] We used motif-x software[17,18] to extract statistically significant motifs from our list of phosphorylation sites (Figure 2C; Tables S1 and Table S2, Supporting Information). In total, we obtained eight pSer motifs, three pThr motifs, and no pTyr motifs. This distribution of motifs is consistent with the percentages of phosphoresidues observed. There were very few pTyr sites, which made it impossible to extract significant motifs, whereas there were many more pSer sites, which made it possible to detect many motifs. The two pThr motifs and four pSer motifs were proline-directed. Two other classes of phosphorylation motifs were identified among the pSer sites: two basic and two acidic. This high diversity of the phosphorylation motifs extracted is consistent with the involvement of a large number of kinases. Indeed, the Pro-directed motifs are specific for MAPK and CDC2; the basic motifs are specific for PKA, PKB, and PKC; and the acidic motifs are specific for the CK2 and ATM kinase groups.[25] The distribution of phosphorylation motif classes differed between TW and OW. Indeed, the acidic pSer motifs were absent, and the basic motif was overrepresented among the phosphorylation peptides most abundant in OW. Moreover, the PPp most abundant in TW contained acidic motifs of a single type (xxxSxxExxx), which suggested that kinases specific for this acidic motif may play an important role in TW formation (Table S1, Supporting Information).

In conclusion, differential phosphorylation events between TW and OW are highly likely; they could occur with kinases, displaying affinity for acidic Ser motifs, active in TW, and kinases, specific for pThr and pTyr, more active in OW.

Distribution of PPp and NPP in SW, TW, and OW

The distribution of identified PPp and NPP in the three types of wood is shown in Figure 3. Most of the PPp (647) and NPP

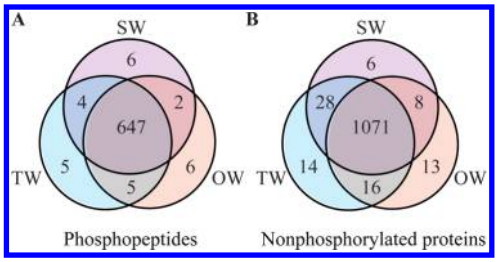

Figure 3. Venn diagram depicting the distribution of the (A) phosphopeptides and (B) proteins found nonphosphorylated identified in the three types of wood: SW, TW, and OW.

(1071) were common to all three types of wood. Surprisingly, TW and SW had 3.5-times more NPP in common than OW and SW (28 and eight NPP, respectively), but this pattern was not observed for PPp (four and two PPp in common, respectively). Some PPp and NPP were in a too low quantity in some MS runs to be detectable. When a peptide was observed only with an additional mass corresponding to one of the isotopic labels, it means that it was very highly differentially abundant between the wood types. In this study, we referred to these peptides as wood-type specific peptides. Looking at the PPp, less than 1% of PPp then were wood-type specific: six PPp were specific to SW, five to TW, and six to OW. Very few NPP were specific to SW (six proteins, corresponding to 0.5% of the proteins detected), whereas 14 proteins (1.1%) were specific to TW, and 13 (1.2%) were specific to OW. The 17 PPp identified in one type of wood are listed in Table 2. Nine of these PPp corresponded to PP already known to be phosphorylated, validating our approach and providing additional grounds for confidence in the identification of the other eight. No annotation was available for less than half the PP. Four of the PP specific to SW were involved in different processes known to involve phosphorylation: the cell cycle (MAD1, a mitotic checkpoint protein), metabolism, and endomembrane trafficking (a mitochondrial carrier, a citrate transporter and a GTPase). In TW, the annotated PP were all associated with the same biological processes: metabolism (a glucosyl transferase), endomembrane trafficking (an auxilin), and the cytoskeleton (actin cross-linking protein). In OW, three protein-binding proteins and one protein involved in metabolism were identified.

The 33 NPP identified in only one type of wood are listed in Table 3. A higher proportion of the NPP than of the PP were annotated, and the annotations were more diverse. Moreover, most of the NPP specific to a single type of wood belonged to functional categories that differed between the three types of wood. Some kinases were identified in TW and OW, but not in SW. The NPP found specifically in TW included four fasciclin-like proteins (Potri.004G210600.1, Potri.009G012200.1, Potri.012G015000.1, and Potri.016G066500.1) previously found in the cell wall in the developing xylem[8,26] and two proteins involved in amino-acid biosynthesis. Most of the NPP found specifically in OW were involved in transcription, protein degradation, and cytoskeleton.

These "tissue-specific" proteins were not included in the quantitative analysis based on ratios of protein abundance between TW and SW or between OW and SW described in the following.

Comparison of Enrichment in GO Terms between PP and NPP Differing in Abundance between TW and OW

We found that 389 PPp and 559 NPP for the global proteome differed in abundance between TW and OW (W_i in models 1 and 2) (Table 1; Tables S3 and S4, Supporting Information).

For each protein in both data sets (293 PP and 559 NPP), the GO annotations of the three classes: cellular component (CC), biological process (BP), and molecular function (MF) were considered. Two statistical analyses of enrichment in GO terms were done; one for both data sets and one for the PP and the NPP more abundant in TW and in OW. These analyses were performed with the singular enrichment analysis (SEA) tool of AgriGO[27] and GO on the *Populus trichocarpa* v3.0 annotation from Phytozome. For the first analysis, Tables S5 and S6 of the Supporting Information show the SEA results obtained for the NPP and PP data sets, respectively. We then used the ReviGO tool[28] to identify representative subsets of the enriched GO-term lists on the basis of semantic similarity measures after the selection of enriched terms with an FDR-adjusted p-value <0.05 (see "REVIGO_analysis" in Tables S5 and S6, Supporting Information). "Translation" was the most frequent BP in the NPP list, and "regulation of signal transduction" was the most frequent in the PP subset. The NPP subset displayed enrichment in CC such as "macromolecular complexes" and "cytoplasmic part". However, SEA identified no significant CC enrichment in the PP list. Finally, "structural molecule activity" and "GTPase activity" were two of the most frequently represented MF terms in the NPP subset, whereas the most frequent GO terms for the PP list related to "protein binding", "lipid and phospholipid binding", and "NTP or enzyme regulator activity".

DOI: 10.1021/acs.jproteome.5b00140
J. Proteome Res. 2015, 14, 3188−3203

Table 2. Phosphopeptides Specifically Identified in One Type of Wood

wood[a]	Ppep[b]	*Pt* transcript name[b]	*At* ortholog	GO or KOG description[c]	ref[d]	peptide sequence[e]
SW	pep507	Potri.003G129200.1	AT1G02260	citrate transporter activity	54	VAA***S***AIAVSPNEEKK
SW	pep544	Potri.012G034300.1	AT5G65770	mitotic checkpoint protein MAD1	21	V***S***EEDFGAEK
SW	pep667	Potri.005G033800.1	AT3G05290	predicted mitochondrial carrier protein		TVL***S***SALLLMIK
SW	pep677	Potri.004G226400.1	AT1G09630	GTPase Rab11	55	SLS***S***EESAPASIKDGK
SW	pep634	Potri.015G011900.2	AT5G53030			SL***S***NLENLGCGEVNSK
SW	pep639	Potri.010G175400.1				QV***S***PASNTSTVVNLAEK
TW	pep577	Potri.016G021500.1	AT1G22380	UDP-glucuronosyl and UDP-glucosyl transferase, metabolism	56	Y***S***CNEWGVGMEIGNNVK
TW	pep200	Potri.010G035100.1	AT1G27100	actin cross-linking protein	21	QESSDSHVT***S***PR
TW	pep431	Potri.010G056200.2	AT1G27850		57	GR***S***LEGGLLFK
TW	pep581	Potri.002G134300.2	AT1G75100	auxilin/cyclin G-associated kinase-related	57	HH***S***APETGSSGKTK
TW	pep678	Potri.001G104200.2	AT1G63520			VSKPNLN***SS***VSSAPSRK
OW	pep612	Potri.014G076500.1	AT2G45720	protein binding		YAVASLASLA***ST***K
OW	pep631	Potri.T173400.3	AT1G10310	oxidoreductase activity, metabolism		VPT***TT***ALGTVSRAAATAAAGGGGGGSK
OW	pep636	Potri.010G113400.1	AT1G71000	heat shock protein binding		CDADPMMDRG***SS***HF***S***LSGWGVYGCG
OW	pep236	Potri.004G032200.2	AT4G05150	protein binding	57	GR***S***EASSIISEVPDYLFGLENSDETK
OW	pep595	Potri.001G458600.1	AT3G12930		58	AV***S***PALSIAGVGAG***T***R
OW	pep680	Potri.002G187300.1	AT1G48300			L***S***LPPNGLGTGKCGVPFR

[a]Wood Type (Wood): SW, straight wood; TW, tension wood; OW, opposite wood. [b]Phosphopeptide (Ppep) number and matching *Populus trichocarpa* transcript name. [c]Gene ontology (GO) or EuKaryotic Orthologous Groups (KOG) description and *Arabidopsis* best hit retrieved from the Phytozome database. [d]References of the studies in which the *Arabidopsis* ortholog was described as phosphorylated, obtained with P3DB software. [e]Peptide sequences and phosphorylated amino acids (bold, italic).

For the second analysis, representative subsets of the enriched GO-term lists were obtained for the PP and NPP from TW and those from OW using ReviGo (Tables S7 and S8, Supporting Information). The two sets displayed different enrichments. Some of the terms found more represented in TW referred to the production of new proteins, whereas those more represented in OW referred mainly to protein catabolism. Indeed, TW enriched terms contained "translation", "biosynthesis" as the BP terms and "structural constituent of ribosome", "structural molecule activity", and "ribosome", "cytoplasm", "macromolecular complex" as CC terms. In OW, the terms found more represented referred to protein catabolism and metabolism: "catabolism", "cellular amine metabolism" as BP terms, "endopeptidase activity", as MF terms, and "proteasome complex" as CC terms. These observations are consistent with the more active cell divisions in TW than in OW, requiring protein synthesis.

Hierarchical Clustering of the TW and OW Phosphoproteome and Global Proteome

Hierarchical clustering based on the significant quantitative differences identified groups of PPp and NPP displaying similar patterns of variations between TW and OW. The clusters were of four major types for both data sets. For PPp (Figure 4A), clusters p2 and p3 contained PPp with very different abundances between wood types. The p2 cluster contained OW-associated PPp, whereas the p3 cluster contained TW-associated PPp. Clusters p1 and p2 contained PPp that were least abundant in the SW (value above the *x*-axis), whereas clusters p3 and p4 contained PPp displaying the opposite pattern. Similar trends were observed for the clusters of NPP (Figure 4B): np2 corresponded to OW-associated proteins, whereas np3 corresponded to TW-associated proteins. Clusters np1 and np2 contained proteins that were least abundant in the SW, whereas clusters np3 and np4 contained proteins that were most abundant in the SW. The proportion of proteins more abundant in TW and OW than in SW was higher for the global proteome (np1, np2) than for the phosphoproteome (p1, p2). Interestingly, 17 proteins with significantly different abundances between the wood types and diverse functions were found in both the phosphoproteome and the global proteome. Twelve of these proteins (listed in the first 12 rows of Table 4) belonged to clusters showing similar pattern of abundance between OW and TW. These proteins included five proteins from clusters n1 and np1 (a constituent of the ribosome, a nucleosome assembly protein, a protein involved in steroid biosynthesis, a S/T kinase and an unknown protein) and seven proteins from clusters p2 and np2 (PtPBA1.2 a subunit of the 20S proteasome, a calmodulin, a GTPase, an unknown protein, and two proteins annotated as RNA-binding and protein-binding proteins, PtGAD.2 a protein involved in secondary metabolite biosynthesis). The other five proteins (last five rows of Table 4) belonged to different clusters: a kinase, a protein-binding protein, two GTPases, and a nucleoside transporter protein.

We then focused on proteins present in particularly large or small amounts in TW or OW and those differing in abundance by a factor of at least two between these two types of wood.

PPp Differing in Abundance between Wood Types

We explored the PPp most strongly over- or underrepresented in a particular type of wood in more detail. The most obvious PPp from this category selected for study were those identified in one type of wood only. These PPp had been removed from the quantitative analyses, as quantification was based on abundance normalized against SW. These PPp were described in the first paragraph of the results section. Table 5 provides information about the PPp identified and quantified in the TW and OW displaying high degrees of enrichment (28 PPp more abundant in TW than in OW) or depletion (20 PPp less abundant in TW than in OW) in a particular type of wood. Some of these PPp with differential abundances identified the same PP (five PP were identified with 2−5 PPp). The PPp corresponding to the same protein were found in the same cluster, but some had very different abundances (pep373 and pep374, fold changes (FC) of 15.79 and 2.41, respectively),

DOI: 10.1021/acs.jproteome.5b00140
J. Proteome Res. 2015, 14, 3188−3203

Table 3. Proteins Found Nonphosphorylated Specifically Identified in One Type of Wood

wood[a]	*Pt* transcript name[b]	*At* ortholog	GO or KOG description[c]
SW	Potri.001G157300.1	AT4G17330	RNA binding
SW	Potri.006G110700.1	AT3G08670	
SW	Potri.008G135100.1	AT1G68060	
SW	Potri.014G169900.1	AT3G07660	
SW	Potri.015G095900.1, Pt-PPD3.1	AT5G50400	hydrolase activity
SW	Potri.018G110100.1	AT5G58040	
TW	Potri.002G034000.1	AT1G19600	possible pfkB family carbohydrate kinase
TW	Potri.004G100900.1	AT1G13340	spindle pole body protein
TW	Potri.004G210600.1, Pt-FLA9	AT5G60490	
TW	Potri.008G062700.1	AT3G55730	DNA binding
TW	Potri.009G012200.1, Pt-FLA8	AT5G60490	
TW	Potri.010G065100.1	AT4G13430	3-isopropylmalate dehydratase
TW	Potri.010G076900.1, Pt-RPS15.2	AT5G09510	structural constituent of ribosome
TW	Potri.011G082800.1	AT5G46180	ornithine aminotransferase, transaminase activity
TW	Potri.012G015000.1, PtrFLA7	AT5G03170	
TW	Potri.016G066500.1	AT5G06390	fasciclin and related adhesion glycoproteins
TW	Potri.017G101100.1	AT3G02260	zinc ion binding
TW	Potri.018G020100.1	AT3G47580	protein binding
TW	Potri.018G096300.1	AT2G24720	glutamate-gated kainate-type ion channel receptor subunit GluR5, transport
TW	Potri.T064400.1	AT1G67000	protein kinase activity
OW	Potri.002G176700.1	AT2G46700	CRK3, protein kinase activity
OW	Potri.003G138200.1	AT4G01070	transferase activity
OW	Potri.005G069400.1	AT1G07710	26S proteasome regulatory complex, subunit PSMD10
OW	Potri.005G252200.1	AT1G20670	protein binding
OW	Potri.007G054900.1	AT5G67470	Rho GTPase effector BNI1 and related formins
OW	Potri.008G213500.1	AT4G16110	regulation of transcription
OW	Potri.010G048200.1, Pt-EIF4.3	AT3G26400	
OW	Potri.010G146200.1		
OW	Potri.010G219800.1	AT3G52270	transcription initiation factor IIF, small subunit (RAP30), ATP binding
OW	Potri.012G140800.1	AT5G23750	remorin
OW	Potri.018G030000.1	AT4G14770	
OW	Potri.018G090300.1, Pt-VHA2.2	AT2G18960	ATPase activity
OW	Potri.019G029400.1	AT3G04160	

[a]Wood type (Wood): SW, straight wood; TW, tension wood; OW, opposite wood. [b]*Populus trichocarpa* transcript name. [c]Gene ontology (GO) or EuKaryotic Orthologous Groups (KOG) description and *Arabidopsis* best hit retrieved from the Phytozome database.

whereas others had very similar abundances (pep378, pep379, FCs of 0.41 and 0.49, respectively).

For comparisons in abundance between TW and OW, the highest FC value obtained was 15.79, whereas the lowest was 0.03 (i.e., 32-fold more abundant in OW than in TW). Most of the highly enriched or depleted PPp (30) came from proteins annotated with highly diverse functional classes. Kinases were particularly numerous among these highly specifically over-represented or underrepresented PP. Five kinases (KEG, a phosphoenolpyruvate carboxykinase, a kinase and two serine/threonine kinases) were more abundant in TW than in OW (2 to 6.37 FC), and one kinase (KING1) was present in much smaller amounts in TW than in OW (Table 5). This observation provides additional evidence for the tissue specificity of kinases. Different PP were annotated as nucleic acid-binding and protein-binding in the two types of wood and were present at greater abundance in the TW than in the OW or vice versa. PP linked to protein degradation (ubiquitin ligase, proteasome) and cell wall synthesis (CESAs) were much more abundant in TW than in OW, whereas the PP more abundant in OW than in TW contained a high proportion of some signaling proteins (calmodulin, remorin). Most PPp with a greater abundance in TW than in OW were also characterized by a higher abundance in TW than in SW, with the notable exception of two kinases (pep403 and pep619). Similarly, all the OW-associated PPp were more abundant in OW than in SW. We also screened for PPp more abundant in tilted tree (TW and OW) than in SW (Table S9, Supporting Information). We identified 27 PPp more abundant in TW than in SW and 18 less abundant in TW than in SW, but the magnitude of these differences was not large (FC of 0.18 to 7.44), as shown in Table 5. Five PP were identified by 2−5 PPp. For four of these PP, the PPp identifying the same protein were from the same cluster. However, for the fifth protein (Potri.004G032200.2), the two PPp (pep234 and pep235) behaved differently than in SW. Overall, 12 PPp were more abundant in OW than in SW (FC of up to 41.39), and 11 were less abundant (FC down to 0.03). Three kinases were found to be less abundant in TW than in SW, and two were found to be less abundant in OW than in TW. Three kinases were found to be more abundant in TW than in SW, whereas none were more abundant in OW than in SW. Surprisingly, most of the PP potentially connected to cell wall formation were present at low abundance in TW (katanin, GTPases, glycosyl transferase, kinesin), and only one of these PP (microtubule-associated protein) was more abundant in TW than in SW. The PP identified as highly abundant in TW including some binding proteins and two proteasome proteins. OW in comparison with SW had low quantity of PP involved in cell division (CDC48.1) and key proteins involved in cell wall formation (cellulose synthase).

In phosphoproteomic studies carried out in *Arabidopsis* (grouped together in the P3DB software), the orthologs of 79% of the PP found to be either highly enriched or depleted in our study had already been reported to be phosphorylated. Thus, 21% of the PP identified here were described in their phosphorylated form for the first time in this study.

NPP Displaying Differences in Abundance between Wood Types

As described earlier for the PP, we also explored the NPP displaying the greatest differences in abundance between TW and OW. The characterization of proteins specific to a single type of wood is presented earlier (see Table 3). The proteins displaying high degrees of enrichment (>2 FC) or depletion (<0.5 FC) between TW and OW are listed in Table 6. Fourteen NPP were more abundant in TW than in OW (FC of up to 11.64), and 20 NPP were more abundant in OW than in TW (with a maximum FC of 16.44; FC of 0.06 between TW and OW). Most of these NPP were annotated, and the functions concerned were highly diverse. Many of these proteins were known to be involved in cell wall formation, endomembrane trafficking, transcription, and stress responses. They were found in both the TW-associated and OW-

DOI: 10.1021/acs.jproteome.5b00140
J. Proteome Res. 2015, 14, 3188−3203

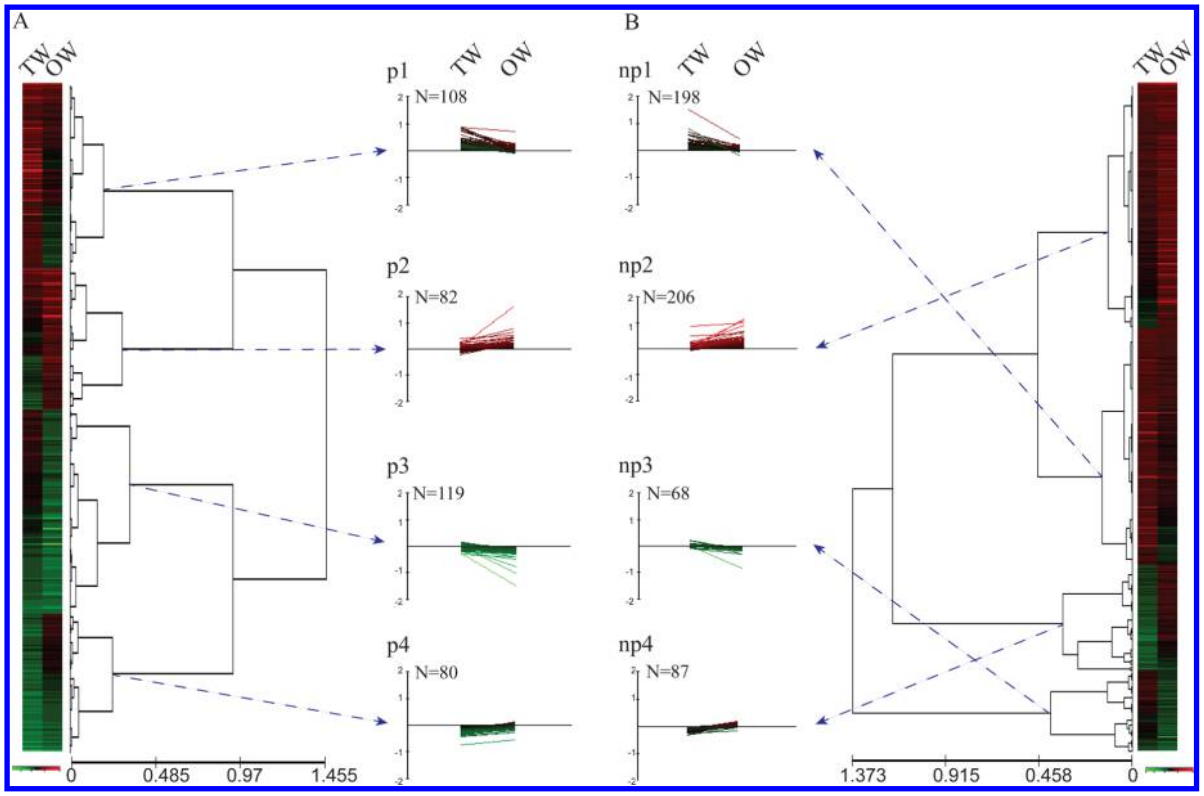

Figure 4. Hierarchical clustering of the (A) phosphoproteome and (B) global proteome of poplar wood-forming tissue. For both data sets (A, phosphopeptides; B, proteins found nonphosphorylated), the log10 ratios of TW/SW and OW/SW were ordered by hierarchical clustering with EPCLUST software (http://www.bioinf.ebc.ee/EP/EP/EPCLUST/). Four main clusters were observed with the phosphopeptides (p1−p4) and the proteins (np1−np4).

Table 4. Proteins Identified in Both the Phosphoproteome and Global Proteome of Poplar Wood-Forming Tissue

Pt transcript name	*At* ortholog	C[b]	GO or KOG description[a]	Ppep[c]	ref
Potri.009G146200.1	AT3G44590	p1 - np1	structural constituent of ribosome	pep224	54
Potri.005G003300.1	AT1G56720	p1 - np1	protein kinase activity	pep467	21
Potri.006G148600.1, NFA902	AT2G19480	p1 - np1	nucleus	pep642	54
Potri.001G376500.1	AT1G53240	p1 - np1	3-beta-hydroxy-delta5-steroid dehydrogenase activity	pep354	21
Potri.019G047600.1	AT5G16730	p1 - np1		pep504	57
Potri.006G077900.1, Pt-PBA1.2	AT4G31300	p2 - np2	proteasome core complex (sensu Eukarya)	pep573	
Potri.001G117900.1	AT1G12310	p2 - np2	calmodulin and related proteins	pep675	
Potri.006G231800.1	AT2G25970	p2 - np2	RNA binding	pep183; 184	
Potri.019G095700.1	AT3G59690	p2 - np2	protein binding	pep23	59
Potri.006G270300.1	AT4G22150	p2 - np2		pep 216	21
Potri.018G076200.1	AT4G13350	p2 - np2	ARF GTPase activator activity	pep319	54
Potri.004G075200.1, Pt-GAD.2	AT5G17330	p2 - np2	glutamate decarboxylase activity	pep107	21
Potri.001G228100.1	AT2G32850	p2 - np4	protein kinase activity	pep395	
Potri.009G080200.1	AT5G64430	p2 - np4	protein binding	pep120; 121	
Potri.003G001400.1, Pt-DH1.2	AT1G59610	p2 - np1	GTPase activity (VPS1)	pep45	59
Potri.019G068700.1	AT1G59610	p3;3;4 - np1	GTPase activity (VPS1)	pep41; 42; 43	59
Potri.006G234100.1	AT5G11710	p4 - np1	equilibrating nucleoside transporter protein	pep275	57

[a]Gene ontology (GO) or EuKaryotic Orthologous Groups (KOG) description retrieved from the Phytozome database. [b]Clusters from the phosphoproteome (p) and the nonphosphorylated proteome (np). [c]Phosphopeptide number.

associated protein classes. Surprisingly, we identified no kinases with a large difference in abundance between TW and OW. As reported above for PP, these NPP were also more abundant in TW or OW than in SW. Large numbers of NPP were found to be more abundant in the TW (16 proteins) and OW (34 proteins) than in the SW. Very few NPP were less abundant in the TW or OW than in the SW (two in TW and three in OW) (Table S10, Supporting Information). These findings are consistent with the larger number of NPP in clusters np1 and np2 than in clusters np3 and np4 (Figure 4B). TW displayed the highest diversity of differences in protein levels with respect to SW, with FC values of 0.46−32.76. In OW, FC values ranged from 0.14−14.23. The proteins concerned had highly diverse functions. One kinase was found to be more abundant in both TW and OW than in SW. Another kinase (Potri.005G003300.1) that was specifically more abundant in

DOI: 10.1021/acs.jproteome.5b00140
J. Proteome Res. 2015, 14, 3188−3203

Publication Date (Web): July 8, 2015 | doi: 10.1021/acs.jproteome.5b00140

Table 5. List of Phosphopeptides More or Less Abundant (FC of at least 2) in TW than in OW[c]

Ppep[a]	*Pt* transcript name[a]	pathway studio[b]	TW/OW	TW/SW	OW/SW	C[d]	GO or KOG description[e]	*At* ortholog	ref[f]	phosphopeptide sequence[g]
pep373	Potri.001G138400.1	DL4895C	15.79	0.50		p3	nucleic acid binding	AT4G17720	58	KMVDDFAQVHLSE*S*PK
pep664	Potri.001G128700.2, Pt-CDC48.1	CDC48B	10.42	1.00		p3	ATP binding	AT2G03670		EPPSSSSGFGGGSSGFGGGG*S*SK
pep523	Potri.014G029800.1	T9J22.24	6.72	6.07		p1		AT2G26570	57	SHVPGSNTETDS*S*PEVKVPR
pep645	Potri.001G280200.1	K15I22.4	6.37	7.44		p1	serine/threonine protein kinase, protein binding	AT4G18640		VVTVKPWATGL*S*GQLQK
pep129	Potri.001G399100.1	F3H9.7	6.00	7.05		p1		AT1G28280	57	DSEPQLLSLFPVT*S*PR
pep126	Potri.011G118200.1	F3H9.7	5.50	5.98		p1		AT1G28281	57	GFYLHP*S*PISTPR
pep347	Potri.004G084000.1	TMK1	5.11	4.12		p1	serine/threonine protein kinase, protein binding	AT1G66150	60	VQ*S*PNEMVIHPR
pep403	Potri.002G107700.2	Os03g0255500	5.03	0.82		p3	phosphoenolpyruvate carboxykinase (ATP) activity	AT4G37870	57	SAPT*T*PIKGAQGAFNAISEEER
pep127	Potri.001G399100.1	F3H9.7	3.79	3.85		p1		AT1G28280	57	LTLSPVTPLNEDPFNKS*S*PSLGNSSEEER
pep358	Potri.004G044100.2	F3H9.11	3.77	5.43		p1		AT1G28240		SG*S*YGSLDK
pep262	Potri.006G200400.2	F11F19.21	3.62	6.17		p1		AT2G35880	21	A*S*HSPLLNQESSNPTK
pep132	Potri.001G399100.1	F3H9.7	2.96	2.40		p1		AT1G28280	57	LTL*S*PVTPLNEDPFNK
pep574	Potri.013G042800.2	F20D21.28	2.75	2.67		p1		AT1G54460	61	SSDDRNSS*S*PSLK
pep131	Potri.001G399100.1	F3H9.7	2.57	3.03		p1		AT1G28280	57	FQETKNP*S*PINSPR
pep439	Potri.009G062600.1	T8G24.6	2.54	1.45		p3	nucleic acid binding, predicted E3 ubiquitin ligase	AT3G08505	62	GS*S*PTSGMDVNSSLR
pep374	Potri.001G138400.1	DL4895C	2.41	1.41		p3	nucleic acid binding	AT4G17720	58	MVDDFAQVHLSE*S*PK
pep204	Potri.002G253200.3	CLASP	2.23	1.77		p1	CLIP-associating protein	AT2G20190	59	SSYDPSDVVG*T*SSEEGYIGASKK
pep235	Potri.004G032200.2	C17L7.70	2.20	2.37		p1	protein binding	AT4G05150	21	TASDVNPGRV*S*Q
pep481	Potri.001G172800.1	F18B13.28	2.19	2.26		p1	protein binding, 26S proteasome regulatory complex	AT1G80210	54	GSELQIS*P*SS*S*RSPR
pep344	Potri.007G096900.1	MNA5.1	2.17	1.28		p3	integral membrane protein	AT5G65290		GSL*S*DDDEDGHGTEIK
pep650	Potri.005G140300.1	F26B6.1	2.14	1.48		p3		AT2G23360		ALA*S*PSEAALFDK
pep334	Potri.005G164000.1	T11I11.17	2.13	2.74		p1	protein binding	AT1G78230	63	VLNQQGGYS*S*DTLELDR
pep31	Potri.006G181900.1, Pt-CESA2.1	PtrCESA7	2.13	1.08		p3	cellulose synthase (UDP-forming) activity	AT5G17420		VHPYPVSEPG*S*AR
pep48	Potri.018G103900.1	PtrCESA7	2.13	1.08		p3	cellulose synthase (UDP-forming) activity	AT5G17420		VHPYPVSEPG*S*AR
pep482	Potri.001G172800.1	F18B13.28	2.08	2.12		p1	protein binding, 26S proteasome regulatory complex	AT1G80210	54	GSELQI*S*PSSSR
pep128	Potri.001G399100.1	F3H9.7	2.07	2.09		p1		AT1G28280	57	NKPEIL*S*PSLLDFPR
pep619	Potri.001G029600.1	KEG	2.04	0.79		p3	protein kinase activity	AT5G13530	57	HLQELPR*S*PPA*S*PDNSFAK
pep240	Potri.003G110000.2	F19I3.28	2.02	1.68		p1	protein kinase activity	AT2G35050	21	VSVQPLAWTE*S*PVR
pep617	Potri.001G324800.1	F4P9.26	0.50		1.43	p2	protein binding	AT2G33490	58	SF*S*IPSSSQR
pep520	Potri.012G140800.1	MRO11.21	0.49		2.78	p2	Remorin family protein	AT5G23750	64	ASE*S*AEEKTEGSVNR
pep379	Potri.004G044800.1	F3H9.7	0.49		2.03	p2		AT1G28280	57	GFYLHP*S*PGSSPRETEPR
pep271	Potri.006G194900.1	AT3G12020	0.49		1.62	p2	kinesin-like protein, microtubule-based movement	AT3G12020	58	LSHPSLAES*S*PSADLLSEVR
pep143	Potri.002G231100.1	EPSIN3	0.48		1.31	p4	equilibrative nucleoside transporter protein, phospholipid binding	AT3G59290	54	KPSEQNIGGPPSYEE*T*ISESRSPAHSER
pep121	Potri.009G080200.1	T12B11.2	0.48		1.87	p2	protein binding	AT5G64430	21	LFLFPVNP*S*PASFGSDGGRSDR
pep82	Potri.010G252500.1	F17F16.16	0.46		1.50	p2		AT1G16860	57	MFIPTEG*S*KSR
pep81	Potri.010G252400.2	F17F16.16	0.45		1.31	p4		AT1G78880	59	KV*S*GPLESTG*S*MK
pep24	Potri.013G127200.3	IQD13	0.45		1.82	p2	protein binding	AT3G59690	59	LSFPLTQGIG*S*FKWNK
pep107	Potri.004G075200.1, Pt-GAD.2	GAD	0.43		1.83	p2	glutamate metabolism	AT5G17330	21	TA*S*ESDVSVHSTFASR

DOI: 10.1021/acs.jproteome.5b00140
J. Proteome Res. 2015, 14, 3188−3203

Table 5. continued

Ppep[a]	*Pt* transcript name[a]	pathway studio[b]	TW/OW	TW/SW	OW/SW	C[d]	GO or KOG description[e]	*At* ortholog	ref[f]	phosphopeptide sequence[g]
pep298	Potri.013G099800.1	F28M11.1	0.43		4.64	p2	RNA binding	AT4G10070		TVSPQPGFPQYDSTQMYAAPR
pep312	Potri.008G177500.1	MNL12.5	0.43		1.27	p4		AT5G43230		KSYASDDELDELDSPMTSIIDNSK
pep675	Potri.001G117900.1	F5O11.35	0.41		2.29	p2	calmodulin	AT1G12310		SIISQENLTAPFDFPR
pep378	Potri.004G044800.1	F3H9.7	0.41		2.60	p2		AT1G28280	57	LLPLFPITSPR
pep398	Potri.011G122100.2	F27G19.50	0.41		1.33	p4		AT4G27450	57	RGSEANWTEWESHS
pep270	Potri.006G194900.2	AT3G12020	0.38		1.06	p4	kinesin-like protein, microtubule-based movement	AT3G12020	58	NISPLASYSQR
pep466	Potri.015G094700.1	KING1	0.36		1.66	p2	protein binding, 5′-AMP-activated protein kinase	AT3G48530	65	VEDLWDVQEPQLSPTEK
pep570	Potri.011G053700.1	F3H9.7	0.34		2.26	p2		AT1G28280	57	LLPLFPVTSPR
pep100	Potri.018G055300.2	F17H15.1	0.33		6.05	p2	RNA binding	AT2G25970		GTYESAPASQTAQQSGVAKASPQS
pep181	Potri.008G182500.2	F3F19.21	0.03		41.39	p2	nucleic acid binding	AT1G13190	57	TRESSYDGDEGASEYGYGEGNHEK

[a]Phosphopeptide numbers (Ppep) and matching *Populus trichocarpa* transcripts. [b]Names used in Pathway studio software for generation of the gene network. [c]TW: tension wood; OW: opposite wood; SW: straight wood. [d]Clusters (C) from the phosphoproteome (p). [e]Gene ontology (GO) or EuKaryotic Orthologous Groups (KOG) description and *Arabidopsis* best hit retrieved from the Phytozome database. [f]References (Ref.) of the studies in which the *Arabidopsis* orthologs were described as phosphorylated, retrieved with P3DB software. [g]Phosphopeptide sequences and phosphorylated amino acids (bold, italic).

TW than in SW was also overabundant in its phosphorylated form (pep467) in the same wood type with respect to SW (Table S9, Supporting Information). This protein was the only protein found to display the same abundance pattern in both data sets. We can hypothesize that the differences in abundance pattern in the presence and absence of phosphorylation resulted from differences in phosphorylation status rather than differences in protein abundance.

DISCUSSION

Trees respond to changes in their equilibrium position by modifying the structure of the wood they produce. TW and OW differ in terms of their structure and chemical composition. A key feature of TW in poplar (as in many angiosperm trees) is the presence of tension wood fibers called G-fibers, in which the secondary cell wall contains a specific layer (G-layer) consisting largely of pure crystalline cellulose microfibrils oriented almost parallel to the axis of the fiber. This layer contributes to the higher proportion of cellulose and lower lignin content in TW than in OW and SW.[7] This characteristic has made TW a versatile model for functional genomics studies of wood formation.[7,29] Fibers are also more numerous and slightly smaller in TW than in OW and SW. These modifications to the structure of the wood in response to a change in the gravitropic status of the tree almost certainly involve the activation of signaling pathways.

Our results indicate that proteins involved in wood formation and signal transduction pathways have differential patterns of abundance in the different types of wood. Many classes of proteins and phosphoproteins were identified in this study. In this section, we chose to focus on those involved in cell wall formation. However, other classes of proteins, for example, proteins playing a role in signal transduction or oxidative stress response, could also be interesting targets for future experiments aiming to better understand the differential mechanisms associated with TW and OW formation. The proteins discussed here display differences in abundances between TW and OW (Tables 5 and 6) or are part of the gene networks shown in Figures S2−S6 of the Supporting Information. In the networks, we referred to the proteins with the short name used in PathwayStudio (*Arabidopsis* or rice homologue and rarely Populus gene names). The correspondences between the Populus name, short name, and *Arabidopsis* best hit given in phytozome are in Tables S11 and S12 of the Supporting Information.

Cellulose

In the three types of wood, five different isoforms of cellulose synthase (CesA) were found either phosphorylated or nonphosphorylated either with large or small differences in abundance between wood types. In *Arabidopsis,* CesA complexes (CSC), consisting of three specific isoforms, are responsible for cellulose synthesis. AtCesA1, AtCesA3, and AtCesA6 are involved in formation of the primary cell wall, whereas AtCesA4, AtCesA7, and AtCesA8 are required for the formation of the secondary cell wall in vascular tissues.[30−32] Some of the isoforms (CesA 1, CesA3, CesA4, CesA7, and CesA8) are required for active complexes, but other subunits are functionally redundant (CesA6 with CesA2, CesA5, and CesA9). In our study, CesA 1, CesA3, CesA4, CesA6, CesA7, and CesA8 were identified and not the redundant isoforms (CesA2, CesA5, and CesA9).

DOI: 10.1021/acs.jproteome.5b00140
J. Proteome Res. 2015, 14, 3188−3203

Table 6. List of Proteins Found Nonphosphorylated More or Less Abundant (FC >2) in TW than in OW[b]

Pt transcript name	pathway studio[a]	TW/OW	TW/SW	OW/SW	C[c]	GO or KOG description[d]	*At* ortholog
Potri.002G078600.1, ACO1	F2P24.4	11.64	32.76		np1	oxidoreductase activity	AT1G77330
Potri.014G016300.1	VDAC2	10.82	6.66		np1	transmembrane transport	AT5G67500
Potri.006G138600.1, Pt-CPN21.1	CPN20	7.17	1.03		np3	protein folding	AT5G20720
Potri.009G087200.1	WLIM1	4.57	3.71		np1	zinc ion binding	AT1G10200
Potri.010G158700.1	T4M8.5	3.79	1.75		np3	prohibitin-related membrane protease subunits	AT2G03510
Potri.016G066600.1	F11F19.21	3.61	4.00		np1		AT2G35880
Potri.006G200400.1	F11F19.21	3.46	5.09		np1		AT2G35880
Potri.014G149900.1	MJE7.13	2.94	2.73		np1		AT5G48490
Potri.014G074600.1	SBTI1.1	2.50	1.66		np3	serine-type endopeptidase activity	AT1G01900
Potri.005G139400.1	AT4G36945	2.46	4.00		np1		AT4G36945
Potri.018G119500.1	Os02g0184200	2.26	2.07		np1	hydrogen-translocating pyrophosphatase activity	AT1G15690
Potri.009G040900.1	PCNA2	2.21	2.36		np1	regulation of DNA replication	AT2G2957
Potri.005G141300.1	K21H1.17	2.13	1.56		np3		AT5G67210
Potri.004G118800.1, Pt-RPS19.1	MAF19.23	2.12	2.52		np1	ribosome	AT3G02080
Potri.014G155200.1	T26B15.8	0.50		2.01	np2	hydrolase activity	AT2G32520
Potri.019G079500.1	PATL2	0.50		1.72	np2	phosphatidylinositol transfer protein SEC14 and related proteins	AT4G09160
Potri.008G161600.1	F5O8.29	0.49		3.15	np2	zinc ion binding	AT1G23740
Potri.003G126100.1, PtrcGpx3_2	GPX6	0.48		2.07	np2	glutathione peroxidase	AT4G11600
Potri.007G092500.2, Pt-ANN1.2	ANNAT2	0.47		1.93	np2	calcium ion binding	AT5G65020
Potri.005G061600.1	PGSIP1	0.47		1.36	np4	transferase activity, plant glycogenin-like starch initiation protein 1	AT3G18660
Potri.015G007300.1	6PGL 4	0.46		2.26	np2	6-phosphogluconolactonase-like protein	AT5G24400
Potri.001G332200.1	AT3G27200	0.44		1.27	np4	copper ion binding	AT3G27200
Potri.008G198600.1, PtrMsrB3	T4B21.5	0.44		1.48	np4	protein-methionine-S-oxide reductase activity	AT4G04830
Potri.006G102400.1, RANBP1	T27E13.20	0.42		2.53	np2	intracellular transport, Ran-binding protein RANBP1	AT5G58590
Potri.005G117500.1, Pt-FAH1.3	FAH1	0.41		1.28	np4	oxidoreductase activity	AT4G36220
Potri.002G257900.1	PtrCESA4	0.40		4.89	np2	cellulose synthase (UDP-forming) activity	AT5G44030
Potri.004G133800.1	F9D12.18	0.38		2.81	np2	ATP binding	AT5G26360
Potri.006G047000.1	SFGH	0.38		2.73	np2	serine-type peptidase activity	AT2G41530
Potri.004G047100.1	DYL1	0.37		3.29	np2		AT1G28330
Potri.006G228600.1	F14F18.60	0.35		1.39	np4		AT5G11890
Potri.004G202800.2	T27G7.6	0.29		4.59	np2	60S ribosomal protein L10A	AT2G27530
Potri.012G037500.1, Pt-RPL19.4	AT3G16780	0.17		8.21	np2	60s ribosomal protein L19	AT1G02780
Potri.008G013200.1, Pt-RPS28.2	RPS28	0.11		12.57	np2	40S ribosomal protein S28	AT5G03850
Potri.018G082900.2	AIM1	0.06		14.23	np2	metabolism	AT4G29010

[a]Names used in Pathway studio software for generation of the gene network. [b]TW: tension wood; OW: opposite wood; SW: straight wood. [c]Clusters (C) from the nonphosphorylated proteome (np). [d]Gene ontology (GO) or EuKaryotic Orthologous Groups (KOG) description and *Arabidopsis* best hit retrieved from the Phytozome database.

The CesA1 and PtCesA3 (CSLD3) isoforms required for primary cell wall formation were found only in their phosphorylated forms. CSLD3 was present in only small amounts in OW (Table S9 and Figure S2, Supporting Information), and CesA1 was more abundant in TW than in OW (Figure S2, Supporting Information). CesA1 phosphorylation modulates cell expansion and the bidirectional mobility of CesAs.[33] Thr166 phosphorylation activates the protein, whereas phosphorylation at other positions, such as Ser167, decreases the activity of the protein.[45] In our study, CesA1 was found to be phosphorylated at this serine residue. Its activity was, therefore, probably inhibited. The high abundance of inactive CesA1 in TW is consistent with the smaller cells produced in this wood type.

Not all the isoforms of the CSC required for secondary cell wall synthesis displayed the same pattern of abundance. None were found in both conformations. CesA8 (PtrCESA8), in its nonphosphorylated form, was more abundant in TW than in OW (Figure S3, Supporting Information), whereas CesA4 (PtrCESA4), also in its nonphosphorylated form, was more abundant in OW than in TW (Table 6). The third subunit of this CesA complex, CesA7 (PtrCESA7), was found only in its phosphorylated form and was more abundant in TW than in OW (Table 5; Figure S2, Supporting Information). Interestingly, the phosphorylation of CesA7 has been shown to target this protein for degradation.[30] This suggests that PtrCESA7 is likely to be more strongly degraded in TW than in OW. Cellulose biosynthesis appears to be strongly regulated at

DOI: 10.1021/acs.jproteome.5b00140
J. Proteome Res. 2015, 14, 3188−3203

various levels. Indeed, as larger amounts of cellulose accumulate in TW than in OW, it has often been suggested that there should be larger amounts of the CesAs involved in secondary cell wall formation in TW than in OW. This hypothesis is consistent with transcription findings for birch TW.[34] However, our results suggest that the presence of the different isoforms is subject to fine control at the translational and post-translational levels.

Cellulose biosynthesis requires UDP-glucose as a substrate of CesA. Carbon fluxes into carbohydrate metabolism are modified as a function of UDP-Glc requirement in the tissues. In TW, the carbon flux seems to be directed into UDP-Glc production, as two sucrose synthases (SUS1 and SUS3) have been shown to be overabundant in this type of wood (Figure S3, Supporting Information). These findings are consistent with the observed greater level of expression of numerous genes of this family in the TW of poplar, hybrid aspen, and birch.[8,34,35] However, other enzymes involved in carbohydrate metabolism via the pentose phosphate pathway or energy production via glycolysis were also found to be more abundant in TW than in OW: a glyceraldehyde 3-phosphate dehydrogenase (Potri.010G055400 referred as Os02g0601300 in the proteins network), a triosephosphate isomerase (Potri.008G056300 referred as Os01g0841600 in the proteins network), a phosphoglycerate kinase (PGK), and a dynamin GTPase (ADL3), all in the nonphosphorylated form (Figure S3, Supporting Information; Table 6). Two Kreb's cycle enzymes, phosphoenolpyruvate carboxykinase (PEPCK, Potri.002G107700 referred as Os03g0255500 in the phosphoproteins network) and malate dehydrogenase (MDH, Potri.001G376500 referred as AT1G53240 in the phosphoproteins network), were found in their phosphorylated form (Figure S2, Supporting Information). In *Saccharomyces cerevisiae*, MDH2 phosphorylation is induced by glucose and inactivates the enzyme.[36] The phosphorylated form of PEPCK is also known to be the less active form.[37] These results therefore suggest that, in TW, more of the carbon flux is allocated to cellulose production than to energy production.

Lignin

Moreover, in TW compared to OW, less carbon flux seems to be directed toward lignin biosynthesis. Lignin is produced in three main steps: the shikimate pathway, which channels the carbon flux from sugar metabolism to phenylalanine production, monolignol biosynthesis, which involves the production of coniferyl and synapyl alcohol from phenylalanine, and monolignol polymerization to build G and S lignin, the two monolignol units constituting the lignin polymer in angiosperms.[38]

In our study, all the classes of monolignol biosynthesis enzymes were less abundant in TW than in OW (Figures S3 and S6, Supporting Information). The enzymes of this pathway, PAL (phenylalanine ammonia lyase, PAL1), followed by C4H (C4HL), C3H (CYP98A3), 4CL (4CL2), HCT (Potri.001G042900 referred as Os04g0500700 in the proteins network), CCoAOMT (PtrCCoAOMT1), CCR (CCR1), F5H (FAH1), COMT (ATOMT1), and CAD (CAD4), leading to the synthesis of coniferyl and synapyl alcohol, were all coordinately less abundant in TW than in OW (Figures S3 and S6, Supporting Information). Since enzymes from these same families are also down-regulated in TW in birch and hybrid aspen,[8,34] no translational regulation appears to occur. Surprisingly, none of the enzymes from the other two parts of the lignin biosynthesis pathway (i.e., shikimate biosynthesis and monolignol oxidative polymerization, the first of these steps occurring before monolignol production and the other occurring after monolignol production) was found to differ in abundance between the different types of wood. This is in agreement with the predictive kinetic metabolic-flux model established by Wang and collaborators, which provides strong evidence that the enzymes of the monolignol pathway are the enzymes that regulate lignin production[39] as opposed to the other steps of the lignin biosynthesis pathway.

Since the lignin content of the TW is known to be lower that of the OW and SW, the lower amount of monolignol enzymes in TW is consistent with a carbon flux oriented to another pathway in this wood type.

G-Layers

As generally observed in woody angiosperm species, the TW fibers of poplar are characterized by the deposition of an additional secondary cell-wall layer, the G-layer. Several studies have shown that the formation of this G-layer in poplar is correlated with the concomitant overexpression of a specific class of arabinogalactan proteins called FLA proteins, for fasciclin-like arabinogalactan proteins.[8,40] FLA proteins have been associated with secondary cell wall or wood formation in several other species, including *Arabidopsis*, cotton, and eucalyptus.[26,41−43] Ten (FLA1−10) of the 15 FLA proteins produced in the xylem are specific to the TW and are not found in the OW.[40] All 10 of these tension wood FLA proteins were recently shown to be downregulated in transgenic poplar plants expressing an FLA6 antisense construct.[34] The transgenic plants displayed modifications to stem biomechanics and cell-wall composition. In our study, only PtrFLA7, PtFLA8, and PtFLA9 were identified (in their nonphosphorylated forms) as specific to the TW (Table 3). Another fasciclin-like protein was also identified (Potri.016G066500.1 similar to AtFLA17/AT5G06390). This is the first time that such a 2-fasciclin-domain FLA protein has been shown to accumulate in TW.

Cytoskeleton and Membrane Trafficking

The relationship between the cytoskeleton and cell wall during cell expansion has been extensively studied (reviewed in ref 44). The cytoskeleton and trafficking pathways act together to control the formation of the cell wall, which consists of networks of polymers. The cytoskeleton plays an important role in the intracellular trafficking of CSC.[45] Indeed, actin is involved in CSC patterning on the plasma membrane through its role in cytoplasmic streaming: it seems to act on both the exocytosis and endocytosis of CSCs.[45,46] Microtubules play a different role, organizing the insertion of CSCs into the plasma membrane.[45,47]

Many components of the cytoskeleton were identified as having different abundances in different wood types. Components of the actin network were particularly abundant in TW. The actin network proteins present in the nonphosphorylated form were actin (ACT11); WLIM1, a protein involved in signal transduction and actin filament organization;[48] VLN4, a villin protein annotated as an actin regulatory protein; and ATGDI1, a small GTPase RAB GDP-dissociation inhibitor involved in membrane trafficking (Figure S3, Supporting Information). Those found in their phosphorylated form were an actin cross-linking protein of unknown function (Potri.010G035100) (Table 2); another villin (VLN4); SPK1, which stabilizes the actin filaments and plays a role in membrane trafficking through the inhibition of EIR1/PIN2

DOI: 10.1021/acs.jproteome.5b00140
J. Proteome Res. 2015, 14, 3188−3203

internalization;[49] and GRL, previously characterized as controlling many actin-based cell shape changes[50] (Figure S2, Supporting Information). However, to our knowledge, nothing is known about the potential role of the phosphorylation of these proteins.

Only one protein (nonphosphorylated) related to actin was found to have a higher abundance in OW than in TW (Table 3; Figure S3, Supporting Information). This protein is a Rho GTPase effector, BIN1 (K919.3/Potri.007G054900), involved in actin polymerization.[51]

Unlike the actin network, for which many phosphoproteins were identified, only one protein from the microtubule network, CLASP, a microtubule-stabilizing protein, was found to differ in abundance between wood types (Figure S2, Supporting Information). Phosphorylated CLASP was more abundant in TW than OW. In vertebrates, the phosphorylated form of CLASP was recently shown to mediate the binding of this protein to microtubules and actin.[52]

Classes of proteins involved in membrane trafficking were identified in TW: VDAC2, involved in transmembrane transport (Table 6), and EPSIN1, involved in clathrin-coated vesicle formation (Figure S3, Supporting Information). The production of this protein is known to be induced by auxin in wood-forming tissue. No auxin biosynthesis or signaling proteins were identified in this study, but the phosphorylated forms of two proteins involved in polar auxin transport (ENP and ARG1) were found to be more abundant in TW than in OW (Figure S2, Supporting Information). ARG1 has recently been shown to be part of a gravity signal transduction pathway in root statocytes, in which it is required for PIN3 relocalization and the asymmetric distribution of auxin in response to gravitational stimulation.[53]

■ ASSOCIATED CONTENT

Supporting Information

The raw MS output files, identified peptides and phosphopeptides, and their corresponding spectra are available in the PROTICdb database at the following address: http://moulon.inra.fr/protic/twphosphoproteo. View of the plants used in the study, sampling technique, and histological observations. Gene network for the phosphoproteins. Gene network for the proteins found nonphosphorylated. Monolignol biosynthesis pathway for proteins found nonphosphorylated. Phosphorylation motifs extracted with motif-x from total phosphopeptides, the phosphopeptides more abundant in TW than in OW, and the phosphopeptides more abundant in OW than in TW. Lists of phosphopeptides ordered by motif category. Statistical analysis of the phosphopeptides quantified in the three types of wood. Probability for phosphosite localization using the Olsen–Mann algorithm (phoscalc). Statistical analysis of the proteins quantified in the three types of wood. Statistical enrichment analysis of GO terms corresponding to the phosphoproteins. Statistical enrichment analysis of GO terms corresponding to the proteins found nonphosphorylated. Statistical enrichment analysis of GO terms corresponding to the phosphoproteins and proteins found nonphosphorylated more abundant in TW. Statistical enrichment analysis of GO terms corresponding to the phosphoproteins and proteins found nonphosphorylated more abundant in OW. Phosphopeptides over- or under-represented (>2-fold change) in one type of wood. Proteins found nonphosphorylated over- or under-represented (>2-fold change) in one type of wood. Correspondences between the Populus phosphoprotein names and their best hit protein. Correspondences between the Populus protein names and their best hit protein. The Supporting Information is available free of charge on the ACS Publications website at DOI: 10.1021/acs.jproteome.5b00140.

■ AUTHOR INFORMATION

Corresponding Author

*E-mail: plomion@pierroton.inra.fr. Phone: +33 (0) 5 57 12 27 65.

Notes

The authors declare no competing financial interest.

■ ACKNOWLEDGMENTS

This study was supported by INRA and the ANR (TROPIC, 11-BSV7-0012).

■ REFERENCES

(1) Cosgrove, D. J. Cellular mechanisms underlying growth asymmetry during stem gravitropism. *Planta* **1997**, *203*, S130–S135.
(2) Fournier, M.; Alméras, T.; Clair, B.; Gril, J. Biomechanical action and biological functions. In *The Biology of Reaction Wood*; Springer Series in Wood Science; Springer-Verlag: Berlin, Heidelberg, 2014; pp 139–169.
(3) Ruelle, J. Morphology, anatomy, and ultrastructure of reaction wood. In *The Biology of Reaction Wood*; Springer Series in Wood Science; Springer-Verlag: Berlin, Heidelberg, 2014; pp 13–35.
(4) Leclercq, A.; Riboux, A.; Jourez, B. Anatomical characteristics of tension wood and opposite wood in young inclined stems of poplar (Populus euramericana cv "Ghoy"). *IAWA J.* **2001**, *2*, 133–157.
(5) Bowling, A. J.; Vaughn, K. C. Immunocytochemical characterization of tension wood: Gelatinous fibers contain more than just cellulose. *Am. J. Bot.* **2008**, *95*, 655–663.
(6) Fagerstedt, K. V.; Mellerowicz, E.; Gorshkova, T.; Ruel, K.; Joseleau, J.-P. Cell wall polymers in reaction wood. In *The Biology of Reaction Wood*; Springer Series in Wood Science; Springer-Verlag: Berlin, Heidelberg, 2014; pp 37–106.
(7) Pilate, G.; Déjardin, A.; Laurans, F.; Leplé, J.-C. Tension wood as a model for functional genomics of wood formation. *New Phytol.* **2004**, *164*, 63–72.
(8) Andersson-Gunneråas, S.; Mellerowicz, E. J.; Love, J.; Segerman, B.; Ohmiya, Y.; Coutinho, P. M.; Nilsson, P.; Henrissat, B.; Moritz, T.; Sundberg, B. Biosynthesis of cellulose-enriched tension wood in Populus: global analysis of transcripts and metabolites identifies biochemical and developmental regulators in secondary wall biosynthesis. *Plant J.* **2006**, *45*, 144–165.
(9) Kaku, T.; Serada, S.; Baba, K.; Tanaka, F.; Hayashi, T. Proteomic analysis of the G-layer in poplar tension wood. *J. Wood Sci.* **2009**, *55*, 250–257.
(10) Plomion, C.; Pionneau, C.; Baillères, H. Analysis of Protein Expression along the Normal to Tension Wood Gradient in Eucalyptus gunnii. *Holzforschung* **2003**, *57*, 353–358.
(11) Plomion, C.; Lalanne, C. Protein extraction from woody plants. *Methods Mol. Biol. Clifton NJ.* **2007**, *355*, 37–41.
(12) Boersema, P. J.; Raijmakers, R.; Lemeer, S.; Mohammed, S.; Heck, A. J. R. Multiplex peptide stable isotope dimethyl labeling for quantitative proteomics. *Nat. Protoc.* **2009**, *4*, 484–494.
(13) Craig, R.; Beavis, R. C. TANDEM: matching proteins with tandem mass spectra. *Bioinformatics* **2004**, *20*, 1466–1467.
(14) Valot, B.; Langella, O.; Nano, E.; Zivy, M. MassChroQ: a versatile tool for mass spectrometry quantification. *Proteomics* **2011**, *11*, 3572–3577.
(15) Benjamini, Y.; Hochberg, Y. Controlling the False Discovery Rate: A Practical and Powerful Approach to Multiple Testing. *J. R. Stat. Soc. Ser. B Methodol.* **1995**, *57*, 289–300.

DOI: 10.1021/acs.jproteome.5b00140
J. Proteome Res. 2015, 14, 3188–3203

(16) Vilo, J.; Kivinen, K. Regulatory sequence analysis: application to the interpretation of gene expression. *Eur. Neuropsychopharmacol.* **2001**, *11*, 399−411.
(17) Chou, M. F.; Schwartz, D. Biological sequence motif discovery using motif-x. *Curr. Protoc. Bioinf.* **2011**, 15−24.
(18) Schwartz, D.; Gygi, S. P. An iterative statistical approach to the identification of protein phosphorylation motifs from large-scale data sets. *Nat. Biotechnol.* **2005**, *23*, 1391−1398.
(19) Nikitin, A.; Egorov, S.; Daraselia, N.; Mazo, I. Pathway studio—the analysis and navigation of molecular networks. *Bioinformatics* **2003**, *19*, 2155−2157.
(20) Liu, C.-C.; Liu, C.-F.; Wang, H.-X.; Shen, Z.-Y.; Yang, C.-P.; Wei, Z.-G. Identification and analysis of phosphorylation status of proteins in dormant terminal buds of poplar. *BMC Plant Biol.* **2011**, *11*, 158.
(21) Sugiyama, N.; Nakagami, H.; Mochida, K.; Daudi, A.; Tomita, M.; Shirasu, K.; Ishihama, Y. Large-scale phosphorylation mapping reveals the extent of tyrosine phosphorylation in Arabidopsis. *Mol. Syst. Biol.* **2008**, *4*, 193.
(22) Bodenmiller, B.; Mueller, L. N.; Mueller, M.; Domon, B.; Aebersold, R. Reproducible isolation of distinct, overlapping segments of the phosphoproteome. *Nat. Methods* **2007**, *4*, 231−237.
(23) Facette, M. R.; Shen, Z.; Björnsdóttir, F. R.; Briggs, S. P.; Smith, L. G. Parallel proteomic and phosphoproteomic analyses of successive stages of maize leaf development. *Plant Cell* **2013**, *25*, 2798−2812.
(24) Wang, X.; Goshe, M. B.; Soderblom, E. J.; Phinney, B. S.; Kuchar, J. A.; Li, J.; Asami, T.; Yoshida, S.; Huber, S. C.; Clouse, S. D. Identification and Functional Analysis of in Vivo Phosphorylation Sites of the Arabidopsis BRASSINOSTEROID-INSENSITIVE1 Receptor Kinase. *Plant Cell* **2005**, *17*, 1685−1703.
(25) Lee, T.-Y.; Lin, Z.-Q.; Hsieh, S.-J.; Bretaña, N. A.; Lu, C.-T. Exploiting maximal dependence decomposition to identify conserved motifs from a group of aligned signal sequences. *Bioinformatics* **2011**, *27*, 1780−1787.
(26) MacMillan, C. P.; Mansfield, S. D.; Stachurski, Z. H.; Evans, R.; Southerton, S. G. Fasciclin-like arabinogalactan proteins: specialization for stem biomechanics and cell wall architecture in Arabidopsis and Eucalyptus. *Plant J.* **2010**, *62*, 689−703.
(27) Du, Z.; Zhou, X.; Ling, Y.; Zhang, Z.; Su, Z. agriGO: a GO analysis toolkit for the agricultural community. *Nucleic Acids Res.* **2010**, *38*, W64−W70.
(28) Supek, F.; Bošnjak, M.; Škunca, N.; Šmuc, T. REVIGO summarizes and visualizes long lists of gene ontology terms. *PLoS One* **2011**, *6*, e21800.
(29) Timell, T. E. The chemical composition of tension wood. *Sven. Papperstidning* **1969**, *72*, 173−181.
(30) Taylor, N. G. Identification of cellulose synthase AtCesA7 (IRX3) in vivo phosphorylation sites–a potential role in regulating protein degradation. *Plant Mol. Biol.* **2007**, *64*, 161−171.
(31) Persson, S.; Paredez, A.; Carroll, A.; Palsdottir, H.; Doblin, M.; Poindexter, P.; Khitrov, N.; Auer, M.; Somerville, C. R. Genetic evidence for three unique components in primary cell-wall cellulose synthase complexes in Arabidopsis. *Proc. Natl. Acad. Sci. U. S. A.* **2007**, *104*, 15566−15571.
(32) Endler, A.; Persson, S. Cellulose Synthases and Synthesis in Arabidopsis. *Mol. Plant* **2011**, *4*, 199−211.
(33) Chen, S.; Ehrhardt, D. W.; Somerville, C. R. Mutations of cellulose synthase (CESA1) phosphorylation sites modulate anisotropic cell expansion and bidirectional mobility of cellulose synthase. *Proc. Natl. Acad. Sci. U. S. A.* **2010**, *107*, 17188−17193.
(34) Wang, C.; Zhang, N.; Gao, C.; Cui, Z.; Sun, D.; Yang, C.; Wang, Y. Comprehensive transcriptome analysis of developing xylem responding to artificial bending and gravitational stimuli in Betula platyphylla. *PLoS One* **2014**, *9*, e87566.
(35) Déjardin, A.; Leplé, J.-C.; Lesage-Descauses, M.-C.; Costa, G.; Pilate, G. Expressed sequence tags from poplar wood tissues–a comparative analysis from multiple libraries. *Plant Biol.* **2004**, *6*, 55−64.
(36) Minard, K. I.; McAlister-Henn, L. Glucose-induced phosphorylation of the MDH2 isozyme of malate dehydrogenase in Saccharomyces cerevisiae. *Arch. Biochem. Biophys.* **1994**, *315*, 302−309.
(37) Walker, R. P.; Chen, Z.-H.; Acheson, R. M.; Leegood, R. C. Effects of Phosphorylation on Phosphoenolpyruvate Carboxykinase from the C4 Plant Guinea Grass. *Plant Physiol.* **2002**, *128*, 165−172.
(38) Poovaiah, C. R.; Nageswara-Rao, M.; Soneji, J. R.; Baxter, H. L.; Stewart, C. N. Altered lignin biosynthesis using biotechnology to improve lignocellulosic biofuel feedstocks. *Plant Biotechnol. J.* **2014**, *12*, 1163−1173.
(39) Wang, J. P.; Naik, P. P.; Chen, H.-C.; Shi, R.; Lin, C.-Y.; Liu, J.; Shuford, C. M.; Li, Q.; Sun, Y.-H.; Tunlaya-Anukit, S.; et al. Complete Proteomic-Based Enzyme Reaction and Inhibition Kinetics Reveal How Monolignol Biosynthetic Enzyme Families Affect Metabolic Flux and Lignin in Populus trichocarpa. *Plant Cell* **2014**, *26*, 894−914.
(40) Lafarguette, F.; Leplé, J.-C.; Déjardin, A.; Laurans, F.; Costa, G.; Lesage-Descauses, M.-C.; Pilate, G. Poplar genes encoding fasciclin-like arabinogalactan proteins are highly expressed in tension wood. *New Phytol.* **2004**, *164*, 107−121.
(41) Qiu, D.; Wilson, I. W.; Gan, S.; Washusen, R.; Moran, G. F.; Southerton, S. G. Gene expression in Eucalyptus branch wood with marked variation in cellulose microfibril orientation and lacking G-layers. *New Phytol.* **2008**, *179*, 94−103.
(42) Dharmawardhana, P.; Brunner, A. M.; Strauss, S. H. Genome-wide transcriptome analysis of the transition from primary to secondary stem development in Populus trichocarpa. *BMC Genomics* **2010**, *11*, 150.
(43) Huang, G.-Q.; Gong, S.-Y.; Xu, W.-L.; Li, W.; Li, P.; Zhang, C.-J.; Li, D.-D.; Zheng, Y.; Li, F.-G.; Li, X.-B. A fasciclin-like arabinogalactan protein, GhFLA1, is involved in fiber initiation and elongation of cotton. *Plant Physiol.* **2013**, *161*, 1278−1290.
(44) Bashline, L.; Lei, L.; Li, S.; Gu, Y. Cell Wall, Cytoskeleton, and Cell Expansion in Higher Plants. *Mol. Plant* **2014**, *7*, 586−600.
(45) Crowell, E. F.; Bischoff, V.; Desprez, T.; Rolland, A.; Stierhof, Y.-D.; Schumacher, K.; Gonneau, M.; Höfte, H.; Vernhettes, S. Pausing of Golgi bodies on microtubules regulates secretion of cellulose synthase complexes in Arabidopsis. *Plant Cell* **2009**, *21*, 1141−1154.
(46) Sampathkumar, A.; Gutierrez, R.; McFarlane, H. E.; Bringmann, M.; Lindeboom, J.; Emons, A.-M.; Samuels, L.; Ketelaar, T.; Ehrhardt, D. W.; Persson, S. Patterning and lifetime of plasma membrane-localized cellulose synthase is dependent on actin organization in Arabidopsis interphase cells. *Plant Physiol.* **2013**, *162*, 675−688.
(47) Gutierrez, R.; Lindeboom, J. J.; Paredez, A. R.; Emons, A. M. C.; Ehrhardt, D. W. Arabidopsis cortical microtubules position cellulose synthase delivery to the plasma membrane and interact with cellulose synthase trafficking compartments. *Nat. Cell Biol.* **2009**, *11*, 797−806.
(48) Khurana, T.; Khurana, B.; Noegel, A. A. LIM proteins: association with the actin cytoskeleton. *Protoplasma* **2002**, *219*, 1−12.
(49) Lin, D.; Nagawa, S.; Chen, J.; Cao, L.; Chen, X.; Xu, T.; Li, H.; Dhonukshe, P.; Yamamuro, C.; Friml, J.; et al. A ROP GTPase-dependent auxin signaling pathway regulates the subcellular distribution of PIN2 in Arabidopsis roots. *Curr. Biol.* **2012**, *22*, 1319−1325.
(50) Zimmermann, I.; Saedler, R.; Mutondo, M.; Hulskamp, M. The Arabidopsis GNARLED gene encodes the NAP125 homolog and controls several actin-based cell shape changes. *Mol. Genet. Genomics* **2004**, *272*, 290−296.
(51) Sit, S.-T.; Manser, E. Rho GTPases and their role in organizing the actin cytoskeleton. *J. Cell Sci.* **2011**, *124*, 679−683.
(52) Engel, U.; Zhan, Y.; Long, J. B.; Boyle, S. N.; Ballif, B. A.; Dorey, K.; Gygi, S. P.; Koleske, A. J.; Vanvactor, D. Abelson phosphorylation of CLASP2 modulates its association with microtubules and actin. *Cytoskeleton* **2014**, *71*, 195−209.
(53) Harrison, B.; Masson, P. H. ARG1 and ARL2 form an actin-based gravity-signaling chaperone complex in root statocytes? *Plant Signaling Behav.* **2008**, *3*, 650−653.
(54) Nakagami, H.; Sugiyama, N.; Mochida, K.; Daudi, A.; Yoshida, Y.; Toyoda, T.; Tomita, M.; Ishihama, Y.; Shirasu, K. Large-Scale

DOI: 10.1021/acs.jproteome.5b00140
J. Proteome Res. 2015, 14, 3188−3203

Comparative Phosphoproteomics Identifies Conserved Phosphorylation Sites in Plants. *Plant Physiol.* **2010**, *153*, 1161−1174.
(55) Pavarotti, M.; Capmany, A.; Vitale, N.; Colombo, M. I.; Damiani, M. T. Rab11 is phosphorylated by classical and novel protein kinase C isoenzymes upon sustained phorbol ester activation. *Biol. Cell Auspices Eur. Cell Biol. Organ.* **2012**, *104*, 102−115.
(56) Zörb, C.; Schmitt, S.; Mühling, K. H. Proteomic changes in maize roots after short-term adjustment to saline growth conditions. *Proteomics* **2010**, *10*, 4441−4449.
(57) Reiland, S.; Messerli, G.; Baerenfaller, K.; Gerrits, B.; Endler, A.; Grossmann, J.; Gruissem, W.; Baginsky, S. Large-scale Arabidopsis phosphoproteome profiling reveals novel chloroplast kinase substrates and phosphorylation networks. *Plant Physiol.* **2009**, *150*, 889−903.
(58) Engelsberger, W. R.; Schulze, W. X. Nitrate and ammonium lead to distinct global dynamic phosphorylation patterns when resupplied to nitrogen-starved Arabidopsis seedlings. *Plant J.* **2012**, *69*, 978−995.
(59) Benschop, J. J.; Mohammed, S.; O'Flaherty, M.; Heck, A. J. R.; Slijper, M.; Menke, F. L. H. Quantitative phosphoproteomics of early elicitor signaling in Arabidopsis. *Mol. Cell. Proteomics* **2007**, *6*, 1198−1214.
(60) Ito, J.; Taylor, N. L.; Castleden, I.; Weckwerth, W.; Millar, A. H.; Heazlewood, J. L. A survey of the Arabidopsis thaliana mitochondrial phosphoproteome. *Proteomics* **2009**, *9*, 4229−4240.
(61) Mayank, P.; Grossman, J.; Wuest, S.; Boisson-Dernier, A.; Roschitzki, B.; Nanni, P.; Nühse, T.; Grossniklaus, U. Characterization of the phosphoproteome of mature Arabidopsis pollen. *Plant J.* **2012**, *72*, 89−101.
(62) Stacey, K. B.; Breen, E.; Jefferies, C. A. Tyrosine Phosphorylation of the E3 Ubiquitin Ligase TRIM21 Positively Regulates Interaction with IRF3 and Hence TRIM21 Activity. *PLoS One* **2012**, *7*, e34041.
(63) Whiteman, S.-A.; Serazetdinova, L.; Jones, A. M. E.; Sanders, D.; Rathjen, J.; Peck, S. C.; Maathuis, F. J. M. Identification of novel proteins and phosphorylation sites in a tonoplast enriched membrane fraction of Arabidopsis thaliana. *Proteomics* **2008**, *8*, 3536−3547.
(64) Marín, M.; Ott, T. Phosphorylation of intrinsically disordered regions in remorin proteins. *Front. Plant Sci.* **2012**, *3*, 86.
(65) Chen, Y.; Hoehenwarter, W.; Weckwerth, W. Comparative analysis of phytohormone-responsive phosphoproteins in Arabidopsis thaliana using TiO2-phosphopeptide enrichment and mass accuracy precursor alignment. *Plant J.* **2010**, *63*, 1−17.

DOI: 10.1021/acs.jproteome.5b00140
J. Proteome Res. 2015, 14, 3188−3203